Resonances, Radiation Pressure, and Optical Scattering Phenomena of Drops and Bubbles

P. L. Marston, S. G. Goosby,* D. S. Langley, and S. E. LoPorto-Arione
Department of Physics, Washington State University, Pullman, Washington 99164

Abstract

Acoustic levitation and the response of fluid spheres to spherical harmonic projections of the radiation pressure are described. Simplified discussions of the $\ell = 1$, 2, and 3 projections are given. A relationship between the tangential radiation stress and the Konstantinov effect is introduced and fundamental streaming patterns for drops are predicted. Experiments on the forced shape oscillation of drops are described and photographs of drop fission are displayed. Photographs of critical angle and glory scattering by bubbles and rainbow scattering by drops are displayed.

Introduction

This paper summarizes research into resonance, acoustical, and optical properties of drops and bubbles. In addition to reviewing earlier work, models concerning tangential stresses, streaming, and the hexapole projection of the radiation pressure are given. These may be applicable to the enhancement of circulation in containerless conditions. New experiments are described. The methodology and notation are simplified from that in earlier papers to manifest the essential results. A review of research into optical properties of bubbles will be published separately[1] so that research is only briefly summarized (near the end of this paper) in a section which may be read independently of the others.

Acoustic Levitation

Experiments on a single drop with a stationary (or nearly so) center-of-mass are possible by counteracting gravitational buoyancy forces with forces due to acoustic radiation pressure. This technique has been particularly useful for obtaining physical properties of metastable liquids (for a review of this application see Ref. 2); however, the present paper is concerned with the mechanics of drops rather than the properties of the constituent fluid. The fluid in the drop is assumed to have a density ρ_i, sound speed c_i, and adiabatic compressibility $\beta_i = (\rho_i c_i^2)^{-1}$. It is assumed to be immiscible in the surrounding host fluid which has corresponding properties c_o, ρ_o, and β_o. The i and o diacritics refer to the inner and outer fluids, respectively. In the diagrams which follow, the z axis is chosen to be up, antiparallel to the acceleration of gravity. The incident acoustic wave (neglecting scattering) will usually be taken to have uniaxial flow parallel to the z axis. The time averaged stresses of the incident and scattered waves not only levitate the drop, they also change its shape.[3] These effects are roughly independent for small deformations and in this section the drop will be assumed to be spherical with a mean radius a with a center at z = 0.

To obtain sufficient radiation pressure forces to counteract buoyancy, the incident sound wave approximates a standing wave, which (for the case of uniaxial flow) has the following pressure $p(z,t) = p_s \cos(kz + kh)\sin\omega t$ where $k = \omega/c_o = 2\pi/\lambda$ and $z = -h$ is the location of an adjacent velocity node. The average force vector on the fluid sphere due to the acoustic radiation pressure (which is second-order in p_s) is[4,5]

$$\langle F \rangle = -\hat{z}(\pi/3)a^3 p_s^2 k(\beta_i - \beta_o D)\sin 2kh, \quad D = (5q-2)/(2q+1), \quad (1a,b)$$

where $\hat{z}$ is the z axis unit vector, q is ρ_i/ρ_o, and the effects of the viscosities of the inner and outer fluids have been neglected. The derivation of Eq. (1) assumes that both $X \equiv ka \ll 1$ and $X \ll X_m$ where $X_m = a\omega_m/c_o$ and ω_m is the lowest radial (or monopole) resonance frequency of the sphere. The latter requirement is due to the omission of the dynamical effects of resonance; in traveling waves these may be included by taking the appropriate case of an expression derived for elastic spheres (see discussion in Ref. 6 of Eq. 24). [It can be shown that the lowest non-zero root of $(1-q)\tan X_i = X_i$ gives $X_m = c_i X_i/c_o$. Drops in liquids with $|1-q| \ll 1$ have $X_i \simeq \pi/2$ and $X_m \simeq \pi c_i/2c_o$. Drops in air have $q \gg 1$, $X_i \simeq \pi$ and $X_m \simeq \pi c_i/c_o$. Gas bubbles have $q \ll 1$ and $X_m \simeq (3\beta_o/\beta_i)^{\frac{1}{2}} \ll 1$.]

The cause of the term proportional to β_i is illustrated in Fig. 1. Assume that $\beta_i \gg \beta_o$ and $\rho_i \lesssim \rho_o$ so that $\beta_i \gg \beta_o D$. For $0 < h \lesssim \lambda/4$, as in Fig. 1, $\langle F \rangle$ is directed downward

---

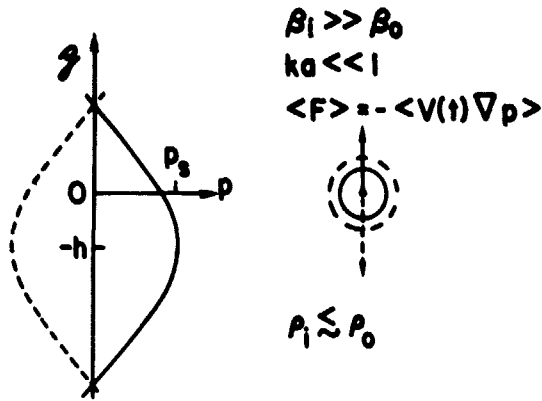*Present address: Naval Undersea Warfare Engineering Station, Keyport, WA 98345.

Fig. 1. The solid and dashed curves illustrate p of the incident wave for $\omega t = \pi/2$ and $3\pi/2$, respectively. Quasi-static responses of the sphere and the associated instantaneous forces due to ∇p are illustrated on the left.
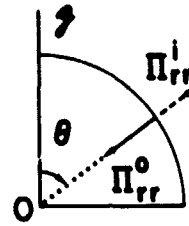
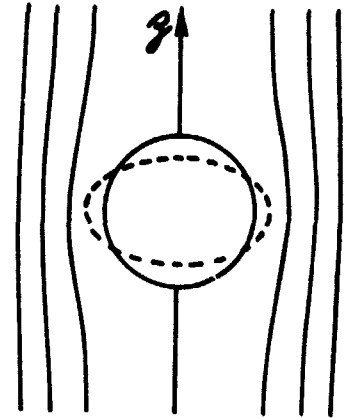Fig. 2. Local mean stresses on a quadrant of the sphere's surface.

Fig. 3. Streamlines for inviscid low frequency flow past a sphere and (dashed) the favored deformation.

since the sphere's volume, $V(t) = (4\pi a^3/3)[1-\beta_i p(0,t)]$, is largest during that part of the cycle when $(-\nabla p)$ is downward; conversely, $\langle F \rangle$ is upward if $\lambda/4 < h < \lambda/2$. In a gravitational field g, there is an equilibrium position where $\langle F \rangle = \hat{z}4\pi a^3(\rho_i-\rho_o)g/3$ provided p_s is sufficiently large. Equilibrium is slightly above a velocity node if $\rho_o < \rho_i$ and slightly below one if $\rho_o > \rho_i$, provided $\beta_o D$ is negligible. For bubbles, $\omega_m = (3/\beta_i \rho_o a^2)^{\frac{1}{2}}$ and if $\omega > \omega_m$ the phase of the response is reversed from that shown in Fig. 1. The direction of $\langle F \rangle$ is reversed so that the bubble is attracted to pressure nodes.[7] There are ordinarily transverse pressure gradients which make the equilibrium unstable in this case.

For drops of hydrocarbon liquids in water, $\beta_i > \beta_o D$ and the equilibrium position is close to a pressure antinode due to the phenomena illustrated in Fig. 1. Levitation apparatus often have a dependence of[2,4,8,9] transverse to the z direction which stabilizes the horizontal position. Typical designs[2,4,8,9] at ultrasonic frequencies require $p_s \approx 2 \times 10^5$Pa. The neglect, implicit in the derivations of Eq. (1), of viscous and thermal effects requires that the viscous (δ_v^i and δ_v^o) and thermal (δ_T^i and δ_T^o) penetration lengths be $<< a$. These are given by $\delta_v = (\nu/\omega)^{\frac{1}{2}}$ and $\delta_T = (\chi/\omega)^{\frac{1}{2}}$ where, for the inner or outer fluid, ν is the kinematic viscosity and χ is the thermal diffusivity. For macroscopic drops the above conditions are satisfied and there is some experimental confirmation[4,10] of Eq. (1).[11] For microscopic objects, e.g., red blood cells, viscous corrections become significant.[11]

For the levitation of liquid or solid spheres in air, $(\beta_i - \beta_o D) \approx -\beta_o 5/2$ and Eq. (1) reduces to the well known expression first derived by King.[12] The sign of $\langle F \rangle$ is reversed and equilibrium positions are near pressure nodes. Attraction to the velocity antinodes occurs because the average reduction in pressure due to the Bernoulli effect is strongest on that side of the drop. Equation (1) neglects harmonics generated from the nonlinearities of the equations-of-state.[13] Harmonic effects can be significant in gases unless they are suppressed.[13]

Multipole Projections of the Radiation Pressure

The radiation pressure on the surface of a compressible sphere is distributed nonuniformly. To describe the response of the sphere, it is convenient to use spherical harmonic (or "multipole") projections of the radial stress

$$R_{\ell m} = \int_0^{2\pi} d\phi \int_0^{\pi} (\Pi_{rr}^i - \Pi_{rr}^o)\tilde{Y}_{\ell m}(\theta,\phi)\sin\theta d\theta, \qquad \Pi_{rr}(\theta,\phi) = 2^{-1}[\beta\langle p_1^2 \rangle - \rho\langle v^2 \rangle] + \rho\langle v_r^2 \rangle \qquad (2a,b)$$

where θ is the polar angle illustrated in Fig. 2; ϕ is the azimuthal angle; p_1, v, and v_r denote the total (incident + scattered) first-order pressure, velocity, and radial velocity; $\langle\rangle$ denotes an average over an acoustic period; and the $Y_{\ell m}$ are real-valued spherical harmonic functions described in Ref. 14.** Equation (2b) evaluated for the conditions at the inner side of the sphere's surface gives the radially outward force/area; evaluated at the

---

**The notation is simpler than in Ref. 14 and 15 since we first consider unmodulated incident waves. Correct prescriptions for the $\tilde{Y}_{\ell m}$ with $\ell \geq |m| \neq 0$ are given in footnote 4 of Ref. 14. Due to an error of transcription in Ref. 15, the sign of the $\langle v_r^2 \rangle$ term was printed incorrectly in Eq. (M2).

outer side, it gives the inward force/area. Hence Eq. (2a) is the projection of the second-order radially outward force/area. Derivations of the stress tensor for Eq. (2b) are cited in Ref. 15. For incident waves characterized by uniaxial flows along the z axis, $R_{\ell m} = 0$ for $m \neq 0$ and the relevant $\tilde{Y}_{\ell 0}$ are just the ordinary $m = 0$ spherical harmonics: $Y_{00} = (4\pi)^{-\frac{1}{2}}$, $Y_{10} = (3/4\pi)^{\frac{1}{2}}\cos\theta$, $Y_{20} = (5/16\pi)^{\frac{1}{2}}(3\cos^2\theta-1)$, and $Y_{30} = (7/16\pi)^{\frac{1}{2}}(5\cos^3\theta-3\cos\theta)$. We retain the m subscript to allow for other incident waves.

For incident waves with no dependence on ϕ (e.g., the uniaxial case mentioned), the continuity of v_r and p_1 (both oscillate at frequency ω) at the boundary give the following local radiation stress on the sphere's surface[14]

$$\Pi_{rr}^i - \Pi_{rr}^o = \frac{(\beta_i-\beta_o)\,p_1^2}{2} + \frac{d_1\rho_o}{2}\,[qa^{-2}<(\frac{\partial\phi_i}{\partial\theta})^2> + <(\frac{\partial\phi_i}{\partial r})^2>] \tag{3}$$

where $d_1 = q-1$, ϕ_i is the inner acoustic velocity potential and the derivatives are evaluated with the radial coordinate $r = a$; Eq. (3) neglects viscous effects. Expressions for p_1 at $r = a$ and the ϕ_i are derived in Ref. 5. If the incident wave is again the standing wave $p(z,t) = p_s\cos(kz + kh)\sin\omega t$, then Eq. (3) is applicable. From Fig. (2) we expect that $<F> = (4\pi/3)^{\frac{1}{2}}a^2R_{10}$; indeed, a laborious computation of R_{10} reproduces Eq. (1) for the same conditions on X even though Eq. (1) was originally derived by a slightly different method of averaging.

To obtain those radiation stresses which favor the spheroidal (or "quadrupole") deformation of a compressible sphere, we used Eq. (3) and found that[15]

$$R_{20} = R_{20}'[1 + X^2(\frac{d_{2,1}}{5} + \frac{q}{d_1^2}(1-b)) + O(X^4)]\sin^2 kh + R_{20}''\cos^2 kh \tag{4}$$

$$R_{20}' = -\frac{3}{5}p_s^2\beta_o(5\pi)^{\frac{1}{2}}d_{1,2}^2, \qquad R_{20}'' = p_s^2\beta_o(5\pi)^{\frac{1}{2}}\frac{X^2}{9d_3}(\frac{5}{7}d_{1,3}(2+d_3) + 3q - (2+q)b + O(X^2)) \tag{5a,b}$$

where $d_1 = d_\lambda/d_\epsilon$, $d_2 = 1 + 2q$, $d_3 = 2 + 3q$, and $b = \beta_i/\beta_o = c_o^2/qc_i^2$. It is assumed that $X = ka \ll 1$ and that $X \ll X_m$. A remarkable feature of Eq. (4) is that if $q \neq 1$ and the sphere is not precisely centered on a velocity node, then $\sin kh \neq 0$ and R_{20} does not vanish as $X \rightarrow 0$ (that is as $\lambda/a \rightarrow 0$). The reason for this is illustrated in Fig. 3. Assume also that $\rho_i \gg \rho_o$ (as for a drop in air) so that translational motion of the sphere is negligible.[1] At the equator ($\theta = 90°$) the mean pressure is less than at the poles since the poles are stagnation points. Consequently, there is an outward directed stress on the equator which will tend to deform a drop into a nearly oblate spheroidal shape as has been observed.[16] The equilibrium shape is determined by a balance of R_{20} with stresses due to surface tension.[14,15] The pressure distribution of oscillating incompressible potential flow[15] has been used to give an independent derivation of Eq. (5a) which does not even require that $\rho_i \gg \rho_o$. This argument has also been extended to traveling waves, where as $X \rightarrow 0$, $R_{20}' \rightarrow R_{20}^o$ with p_s equal to the pressure amplitude of the incident wave. The only $R_{\ell m}$ which do not necessarily vanish as $X \rightarrow 0$ have $\ell = 2$ or $\ell = 0$.

Compressible liquid drops (e.g., silicone oil or xylene) in water are attracted toward velocity nodes where the part of $R_{20} \propto \sin^2 kh$ is small and R_{20} is dominated by R_{20}''. For these drops R_{20}'', and hence R_{20}, are negative numbers because $(2+q)b$ dominates the other terms in the parentheses in Eq. (5b). The tendency is again to deform into an oblate spheroid but for a different reason than that depicted in Fig. 3; it appears that the attraction depicted in Fig. 1 of compressible fluids to the velocity node can also deform a drop. If a drop with $\beta_i > \beta_o$ is somehow constrained (e.g., with the radiation pressure of a second wave) to lie near a pressure node, the term of Eq. (4) $\propto X^2\sin^2 kh$ may be dominant if X^2 is not too small. Then R_{20} is positive and the drop will tend to elongate. This is apparently due to the repulsion of highly compressible fluids from pressure nodes by the mechanism depicted in Fig. 1.

To obtain the hexapole projection, which favors a "pear" shaped deformation of a compressible sphere, we used Eq. (3) and found that $R_{30} = -p_s^2\beta_o(\pi/7)^{\frac{1}{2}}X\,[(3qd_1/d_2d_3) + O(X^2)]\sin 2kh$. It is assumed that $X \ll 1$ and that $X \ll X_m$. The dependences on kh and X differ from those of R_{20} but the periodicity in h may be argued from elementary considerations.

Equation (2) and these results for R_{20} and R_{30} neglect the previously mentioned harmonic effects[13] which are known to alter the $<F>$ exerted on spheres in air when the fundamental amplitude, p_s, is large. Harmonic effects should be negligible when the outer fluid is liquid or, if it is a gas and p_s is small.
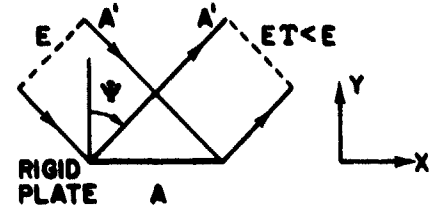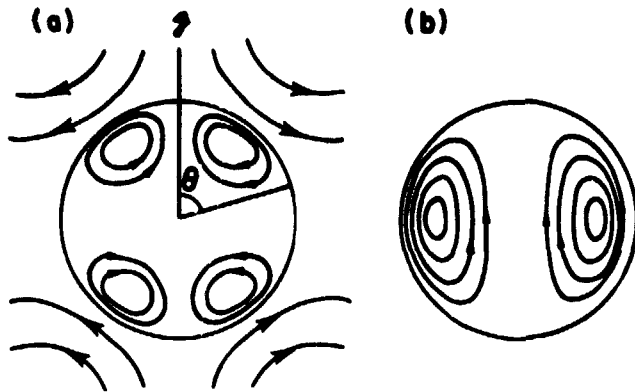
Fig. 5. Streaming patterns driven by projections of $\nabla \cdot T$ with (a) $\ell = 2$, $m = 0$, and (b) $\ell = 1$, $m = 0$.
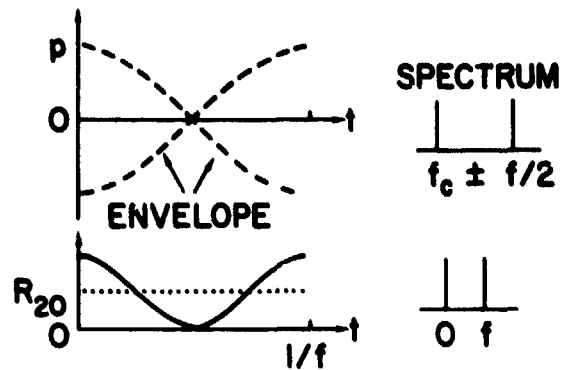
Fig. 6. An appropriate modulation of p gives equal oscillating and static terms in the $R_{\ell m}$.

Tangential Radiation Stresses, the Konstantinov Effect, and Streaming

Let $T = \hat{\theta}\Pi_{\theta r} + \hat{\phi}\Pi_{\phi r}$ denote the time-averaged tangential force vector per area of an infinitesimal region of surface on a compressible sphere. Here $\hat{\theta}$ and $\hat{\phi}$ denote the local unit vectors (at the surface point specified by θ and ϕ) in the direction of increasing polar and azimuthal angles, respectively. The stress T is taken here to denote the total radiation stress due to the inner and outer (incident + scattered) acoustic waves. Marston has shown[14] that T vanishes if the first-order (or acoustic) flow is assumed to be adiabatic-inviscid (or "potential") flow. Viscous or thermal dissipation near the sphere's surface produces tangential stresses. The purpose of this section is to comment on these stresses and on the associated acoustic streaming.

The connection between dissipation and tangential stress is illustrated by the "thought experiment" shown in Fig. 4. A sound beam with a mean energy density E and area A' is reflected off a rigid plate of area $A = A'/\cos\Psi$. The reflected beam has mean energy density TE where $T < 1$. The y coordinates at which these energy densities are specified are much greater than the viscous and thermal penetration lengths for the fluid, δ_v and δ_τ. Attenuation due to any absorption in the bulk fluid (which leads in part to "volume" acoustic streaming) is neglected here so that T is associated with the losses localized within the region extending a few penetration lengths from the plate. The incident and reflected waves have pseudomomentum densities[17] of E/c and TE/c where c is the fluid's sound speed. Time rates-of-change of the incident and reflected pseudomomenta (in their respective directions of propagation) are EA' and TEA'. The plate feels a tangential radiation force in the x direction equal to the rate of x-pseudomomentum loss, $(1-T)EA'\sin\Psi$. Consequently the tangential radiation stress $\Pi_{xy} = E(1-T)(A'/A)\sin\Psi = (E/2)(1-T)\sin 2\Psi$. For an inviscid fluid, $T = 1$ and $\Pi_{xy} = 0$ at a rigid plate. An equation similar in form to this expression was derived by Börgnis[18] in a different context. He neglected the possibility of viscous and thermal boundary layers but attributed $(1-T)$ as due to refracted waves within the (now elastic) reflector in an inviscid fluid. That interpretation would require that the refracted waves are absorbed within the plate. Also it neglects dissipation external to the plate.

A theory for the dependence of the intensity reflection coefficient T on the angle of incidence Ψ was given by Konstantinov[19] for a rigid plate maintained at a fixed temperature. For the purpose of estimating the dependence of Π_{xy} on Ψ and its maximum value Π_{xy}, our numerical tests show that the following approximation (Ref. 20, Eq. 1) to Konstantinov's T (see Ref. 19, Eq. 53) is applicable

$$T \simeq (\Psi_1^2 + \Psi_2^2 - 2^{\frac{1}{2}}\Psi_1\Psi_2)/(\Psi_1^2 + \Psi_2^2 + 2^{\frac{1}{2}}\Psi_1\Psi_2) \qquad (6)$$

where $\Psi_1 = (\pi/2) - \Psi$ radians is frequently called the "grazing angle" and $\Psi_2 = \Psi_v + \Psi_\tau$ where $\Psi_v = k\delta_v$ and $\Psi_\tau = (\gamma-1)k\delta_\tau$. Here δ_v and δ_τ are the penetration lengths of the surrounding fluid as previously defined and γ is the ratio of specific heats at constant pressure and volume. There is a minimum T of $(2^{\frac{1}{2}} - 1)^{\frac{1}{2}} \simeq 0.176$ which occurs for $\Psi_1 = \Psi_2$. Unless the acoustic frequency $f = \omega/2\pi$ is quite large ($\gtrsim 1$ GHz), most fluids have $\lambda \gg \delta_v$ and $\lambda \gg \delta_\tau$ so that the minimum in T usually occurs for Ψ near 90°. For most liquids $\Psi_v \gg \Psi_\tau$ and the thermal boundary condition is not important.

In the following discussion of T and its influence on Π_{xy}, it should be remembered that for a given fluid, $\Psi_2 \propto \sqrt{f}$. Consider the cases of air and water at a temperature of 20°C and $f = 1$ MHz: for air, $\delta_v = 1.5$ µm, $\delta_\tau = 1.8$ µm, and $\Psi_2 = 2.4°$; for water, $\delta_v = 0.4$ µm, $\delta_\tau = 0.15$ µm, and $\Psi_2 = 0.10°$. Numerical computations give $\Pi_{xy} \propto \Psi_2$ with $\Pi_{xy} = 0.043$ E when
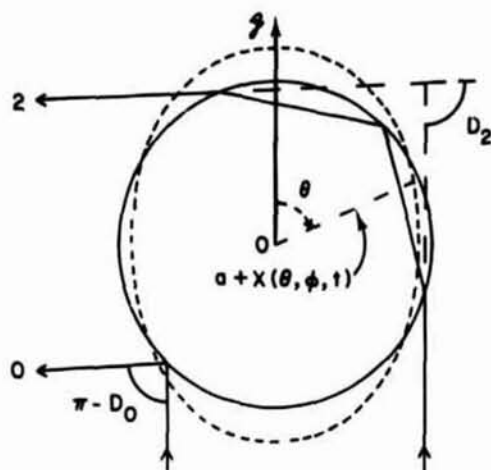
169

Fig. 7. Rays for a spherical drop of xylene in water which contribute to rainbow scattering. The dashed profile is when $x_{\ell m}(t) > 0$, $\ell = 2$, $m = 0$.

Fig. 8. Far-field scattering for: (a) the rainbow region of a xylene drop (a≈200 µm) levitated in water; and (b) the critical region of an air bubble (a≈480 µm) in water. In both cases the incident light had a wavelength (in water) of 632.8 nm/n_0 where $n_0 \approx 1.33$. In (a) the scattering angle (denoted by D in Fig. 7) increases from left to right; the angular width of the photograph 7°. The coarse structure (broad vertical bands) is described by Airy's diffraction integral. In (b) the scattering angle (ϕ in Fig. 11) decreases from left to right (with ϕ_c near the left edge) and the width ≈14°. The coarse structure in (b) is due to critical diffraction and interference. The scattering plane and the incident electric field are perpendicular in (a) and parallel in (b).

$\Psi_2 = 1°$. The sin2Ψ factor in Π_{xy} causes Π_{xy} to occur with $\Psi_1 > \Psi_2$. (The Ψ_1 associated with $\Pi_{xy}^{\dagger}$ approaches 8° as $\Psi_2 \to 0$; it increases with increasing Ψ_2 with a slope of roughly 8 until $\Psi_2 = 1°$ and more slowly thereafter.) The maximum in Π_{xy} is broad; $\Pi_{xy}(\Psi = 45°) \approx 0.03$ E when $\Psi_2 = 1°$ and $\Pi_{xy}(45°)$ is roughly $\propto \Psi_2$. For $\Psi \le 70°$, Konstantin's T depends somewhat on Ψ_ν/Ψ_τ; however, this dependence is not retained in Eq. (6) and in these estimates.

Herrey[21] has measured radiation stresses on a copper plate in water but did not detect tangential stresses for $f = 1$ MHz and $\Psi \le 50°$. It may be that for these Ψ the experiment was not able to discriminate between the Π_{xy} and the much larger normal stress whose magnitude = 2 E when $\Psi = 0$. Second-order acoustic torques on a rigid surface caused by tangential stresses have been observed.[22]

It might appear that the expression for Π_{xy} does not allow for the momentum of fluid streaming near the surface. If the extent of the plate is lengthened, however, so that viscosity transfers the x-momentum of the second-order flow to the plate, the apparent Π_{xy} on the plate is still given by this expression. This may also be shown by considering the momentum flux across a control surface which encloses both the plate and the confined streaming. One procedure for describing how the first-order velocity v is coupled to the second-order velocity u is to consider the equation for the second-order vorticity:[23]

$$(\frac{\partial}{\partial t} - \nu\nabla^2)\nabla\times u = -\nu(S_E + S_R + S_T), \quad S_R = -\nu^{-1}<\nabla\times(v\times\nabla\times v)>, \quad S_T = -\beta<\nabla\times(p_1\nabla\times\nabla\times v)> \quad (7a,b,c)$$

where S_E is Eckart's "volume" source of vorticity[23] which is negligible near the surface in comparison to the "surface" sources S_R and S_T. This procedure is useful for the description of streaming near rigid surfaces provided the Reynold's number (for u) is small.

An approximation for u which should be useful near the fluid-fluid interface of a drop or a bubble was introduced by Marston.[14] It is to neglect the source terms in Eq. (7a) and to solve the resulting homogeneous vorticity equation subject to boundary conditions which include the tangential (T) and radial ($R_{\ell m}$) radiation stresses on the interface. As reviewed subsequently, this procedure is particularly useful for describing the response to oscillating $R_{\ell m}$ due to modulated sound. In this section the sound has no modulation and u is driven only by the T. By inspection of Eq. (7) and extension of the previous momentum arguments, this procedure should be useful if the spatial extent of the region of significant $|\nabla\times v|$ is << a; this will be so if δ_ν << a which is usually the case of interest. The resulting u can be written in a series which makes use of multipole projections $(\nabla\cdot T)_{\ell m}$ of the tangential divergence of T [see Eq. (14) and Appendix B of Ref. 14]. As noted previously,[15] for steady flows the coupling coefficients in Ref. 14 were incorrect due to errors in the assumed boundary conditions (Ref. 14, Eq. C6 and C10). These errors have been corrected in the result given below. For incident acoustic waves with no ϕ dependency $\Pi_{\phi r} = 0$ and $\Pi_{\theta r}$ is independent of ϕ. This T(θ) must be present because of the dissipation of sound present at interfaces separating real fluids.[20] Its description may be facilitated with methods developed for torques.[22]

Consider the particular case of $\Pi_{\theta r} = B_2 \sin 2\theta$ where B_2 is a constant. This $\Pi_{\theta r}$ has $(\nabla\cdot T)_{20} = 8(\pi/5)^{\frac{1}{2}} B_2/a$ and all other $(\nabla\cdot T)_{\ell m} = 0$ as does the torque. The interface is
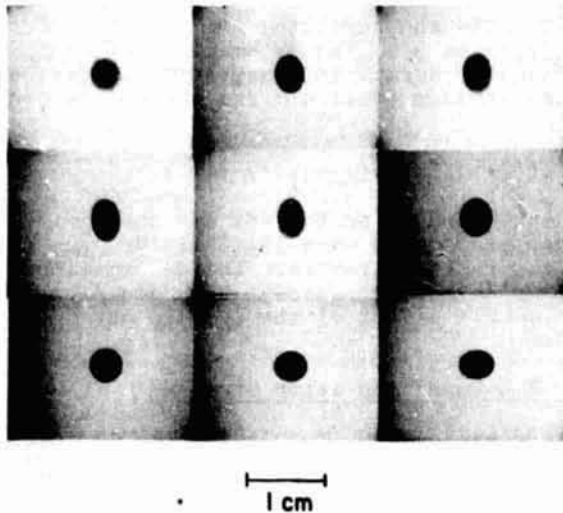
Fig. 9. A 2 mm radius drop undergoing forced quadrupole oscillations with f = 18 Hz. Here and in Fig. 10, time increases from left to right and from top to bottom.
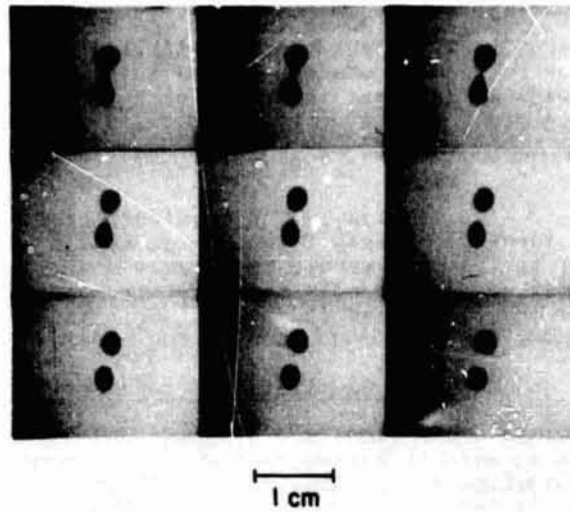
Fig. 10. A 1.7 mm radius drop splitting into two drops as a consequence of forced quadrupole oscillations with f = 24 Hz. Here, and in Fig. 9, the z axis is vertical.

assumed to be ideal (free of surface viscosity) and the boundary conditions are continuity of normal and tangential velocities and the balance of forces. These give the following velocities inside (i), and outside (o), the sphere: $u_\theta^i = (G\tilde{r}/2)(5\tilde{r}^2-3)\sin 2\theta$, $u_r^i = G\tilde{r}(1-\tilde{r}^2)(3\cos^2\theta-1)$, $u_\theta^o = G\tilde{r}^{-4}\sin 2\theta$ and $u_r^o = G\tilde{r}^{-4}(1-\tilde{r}^2)(3\cos^2\theta-1)$ where $\tilde{r} = r/a$, $G = B_2 a/5(\mu_i + \mu_o)$, and μ is the shear viscosity of the indicated fluid. Resulting streamlines are illustrated in Fig. 5(a). In addition to acoustic stresses, externally applied electric fields[24] can cause tangential stresses with this dependence on θ. With an appropriate choice of material parameters, and B_2, we find that u and the radial stresses caused by u (described in the next section) agree with those predicted by Taylor's specialized method after correcting his algebraic errors.[25] The outer fluid is unbounded in this computation.

Consider now the case of $\Pi_{\theta r} = B_1 \sin\theta$ where the only $(\nabla \cdot T)_{\ell m} \neq 0$ has $\ell = 1$ and $m = 0$. This stress is predicted to drive the following velocity field: $u_\theta^i = G(2\tilde{r}^2-1)\sin\theta$, $u_r^i = G(1-\tilde{r}^2)\cos\theta$, $u_\theta^o = (G/2)\tilde{r}^{-3}(1+\tilde{r}^2)\sin\theta$, and $u_r^o = G\tilde{r}^{-1}(\tilde{r}^{-2}-1)\cos\theta$ where $G = B_1 a/3(\mu_i + \mu_o)$. Interior streamlines are shown in Fig. 5(b); they are the same as those for small Reynolds number flow past a drop calculated by Hadamard and observed by Spells.[26] Far outside the drop, the streamlines are those for a stokeslet, which is the creeping motion generated by a force concentrated at a point (see Fig. 5 of Ref. 27). This type of tangential stress will alter the net z directed force on a sphere from that given by Eq. (1).

For a large drop with $\beta_i \ll \beta_o$ in an incident wave with $X \gg 1$, Eq. (6) and the considerations illustrated in Fig. 4 may be used to obtain the signs of B_1 and B_2. If a traveling wave is incident from above, it is clear that $B_1 > 0$ due to the Konstantinov effect. In a standing wave it is to be expected that $B_2 > 0$ due to stress concentrations between $\theta = 45°$ to $85°$ in opposition with those between $95°$ to $135°$; however B_2 should also depend on h. In either case, $B_1 \propto p_s^2$ and $B_2 \propto p_s^2$ unless the incident pressure amplitude p_s is large. [As with acoustic torques,[22] $\Pi_{\theta r}$ may contain a term $\propto p_s$ when the first order displacement amplitude $(p_s/\rho c \omega) \gtrsim \delta_v$.] The total u will be the superposition of those driven by the individual $(\nabla \cdot T)_{\ell m}$.

Deformations Induced by Steady Radiation Stresses

Radiation stresses induce a mean displacement of the interface of a drop or bubble which is opposed by surface tension. The mean displacement (averaged over a period of the acoustic wave) of the interface from that of a sphere of radius a will be denoted as $x(\theta,\phi,t)$ and may be described using the following spherical harmonic series:

$$x(\theta,\phi,t) = x_0(t) + \sum_{\ell=1}^{\infty} \sum_{m=-\ell}^{\ell} [\hat{x}_{\ell m} + x_{\ell m}(t)]\tilde{Y}_{\ell m}(\theta,\phi) \tag{8}$$

where $\hat{x}_{\ell m}$ is a time-independent projection and $x_{\ell m}$ is an oscillating one. The latter vanishes if the wave is not modulated and initial transients are allowed to decay. It will be assumed in this section that $|x(\theta,\phi,t)| \ll a$ so that for drops the term[14] $|x_0(t)|$ is much smaller than the largest $|\hat{x}_{\ell m}|$. The $\ell = 1$ terms represent translations of the sphere's center which lead to the balance between <F> and buoyancy. The terms representing static

deformations, the $\hat{x}_{\ell m}$ with $\ell > 1$, are proportional to the radiation stresses on a sphere given by Eq. (2) (which neglect the deformation) provided the resulting $|\hat{x}_{\ell m}| << a$. [Corrections to the first-order scattering when $X << 1$ will be $O(\hat{x}_{\ell m}/a)$ or smaller and will induce only small changes in the stresses.] A balance of normal and tangential radiation stresses at an ideal interface with those due to the surface tension σ and the second-order flow gives

$$\hat{x}_{\ell m} = [a^2/\sigma(\ell-1)(\ell+2)][R_{\ell m}-3a(\nabla\cdot T)_{\ell m}\hat{\Gamma}/\ell(\ell+1)(2\ell+1)(\mu_o+\mu_i)], \quad \ell > 1, \qquad (9)$$

where $\hat{\Gamma} = \ell\mu_o+(\ell+1)\mu_i$. The magnitude of T can be estimated using Eq. (6) and the expression for Π_{xy}. Unless f is so high that $\delta_v \not< \lambda$, one expects to have $|R_{\ell m}|>>|a(\nabla\cdot T)_{\ell m}|$ for $\ell > 1$ so that $\hat{x}_{\ell m}$ should be largely determined by the radial stresses. The deformations $\hat{x}_{\ell m}$ may easily exceed[14] the first-order particle displacements ($p_s/\rho c\omega$); they are $\propto p_s^2$ provided $|\hat{x}_{\ell m}| << a$ and $(p_s/\rho c\omega) << \delta_v$. The most noticeable effect of the $(\nabla\cdot T)_{\ell m}$ may be the second-order flow described in the previous section.

Shape Oscillation Resonances Forced by Modulated Radiation Stresses

Second-order flows and deformations may be greatly enhanced by modulating the incident acoustic wave at a frequency so as to force shape oscillation resonance. The purpose of this section is to summarize the theory.[14,15] There is a slight change of notation from the previous sections: f_c will denote the frequency of the incident sound in the absence of modulation (typically $f_c \gtrsim 100$ kHz), and f (which is $<< f_c$) denotes the frequency of the shape oscillations. To drive the shape oscillations, the incident wave is a standing wave of the following form $p(z,t) = -2p_c\sin(\omega_c t)\cos(\frac{1}{2}\omega t)\cos(kz+kh)$ where $\omega_c = 2\pi f_c$, $k = \omega_c/c_o$, $\omega = 2\pi f$, and $z = -h$ is again the location of the adjacent velocity node with $z = 0$ at the drop's center of mass. The factor (-2) is included only as a matter of convention.[14,15] That nonlinearities are essential to the generation of the low frequency shape oscillations is illustrated in Fig. 6. The upper part shows the modulation envelope and the spectrum of the incident sound which consists of two sidebands, each with an amplitude p_c, located at $f_c-(f/2)$ and $f_c+(f/2)$. The wave at the carrier frequency f_c is suppressed, due to the modulation. From Eq. (2) it can be shown[15] that the radiation stresses vary in time such that $R_{\ell m}(t) = \hat{R}_{\ell m}[1+\cos(\omega t)]$ and this has a time dependence and spectrum illustrated in the lower part of Fig. 6. The radiation stress contains a static term and one which oscillates at the difference frequency of the sidebands. The constant $\hat{R}_{\ell m}$ is given by the $R_{\ell m}$ associated with a steady incident wave of frequency f_c and pressure amplitude $p_s = p_c\sqrt{2}$. Consequently Eq. (4) and the result for R_{30} may be used here but with a simple substitution. For small p_c, the tangential stress T will also be proportional to $p_c^2[1+\cos(\omega t)]$.

The theory for the response[14,15] is complicated by the nature of the boundary layer damping. In the present treatment we simplify the results by omitting the small deformation and flow induced by the oscillating part of $(\nabla\cdot T)_{\ell m}$. For incident waves with no dependence on ϕ, all projections with $m \neq 0$ vanish. Consequently the subscript m will be omitted. The oscillating parts of Eq. (8) are given by

$$x_\ell(t) = \tilde{x}_\ell\cos(\omega t-\xi), \quad \tilde{x}_\ell = \hat{x}_\ell\omega_\ell^{*2}/(U^2+V^2)^{\frac{1}{2}}, \quad \tan\xi = V/U, \quad \ell > 1, \qquad (10a,b,c)$$

$$\omega_\ell^* = [\sigma\ell(\ell+1)(\ell-1)(\ell+2)/a^3\Gamma]^{\frac{1}{2}}, \quad U(\omega) = \omega_\ell^{*2}- \alpha\omega^{3/2}-\omega^2, \quad V(\omega) = \alpha\omega^{3/2}+\gamma\omega \qquad (11a,b,c)$$

and the static parts, $\hat{x}_\ell$, are given from Eq. (9) by omitting the $(\nabla\cdot T)$ term. In Eq. (11a) ω_ℓ^* is the natural frequency (neglecting viscosity) of the ℓth mode and $\Gamma = \ell\rho_0+(\ell+1)\rho_i$. Here α and γ are damping parameters [given by Eqs. (22) and (23) of Ref. 14] which are functions of ℓ, a, μ_i, μ_0, ρ_i, and ρ_0; α is due to the damping of the boundary layer since it vanishes if either $\rho_i\mu_i \to 0$ or $\rho_0\mu_0 \to 0$. For drops surrounded by a liquid, γ is typically $< \alpha\omega^{*\frac{1}{2}}$ but it is similar in magnitude to α^2. It was assumed in the theory for α and γ that the interface was ideal and thus free of surfactants.

From Eq. (10b), $\tilde{x}_\ell$ depends both on the frequency and ℓth projection of the stress. As quantified below, when ω is slightly less than ω_ℓ^*, $|x_\ell|$ is maximized; depending on the stress distribution, other modes may be driven but at lower (nonresonant) amplitudes. An example of a pure $\ell = 2$ profile is shown in Fig. 7. It is convenient to omit the ℓ subscript when possible in the following discussion. The phase delay of oscillations ξ is 90° when ω is chosen to be the quadrature frequency $\bar{\omega}$. The prediction is that $U(\bar{\omega}) = 0$ which gives $\bar{\omega} = \omega^* - (\alpha/2)\omega^{*\frac{1}{2}} + \alpha^2/4$. Due to the inertia of the boundary layer,[14] $\bar{\omega} \neq \omega^*$, unlike the case of ordinary damping. The mechanical Q of the ℓth mode is $\simeq \omega^{*2}/V(\omega^*)$ provided μ_i and μ_0 are small enough to make this ratio somewhat larger than unity. [Evidently $\bar{\omega} \simeq \omega^*(1-\frac{1}{2}Q^{-1})$ for liquid-liquid systems.] The response amplitude $|\tilde{x}|$ is maximized when $\omega \simeq \bar{\omega}$. At this maximum, $\tilde{x} \simeq Q\hat{x}$, so the oscillations should be enhanced by a factor of Q. As $\omega/\omega^* \to 0$, $\tilde{x} \to \hat{x}$; however, as $\omega/\omega^* \to \infty$, $\tilde{x}/\hat{x} \to 0$.

A matrix, Eq. (17) of Ref. 14, makes it possible to compute the oscillating part u. (The

total u also contains a static part driven by the static part of T.) In this matrix and in Eqs. (7), (9), (10), and (11), convection of momentum by the second order flow was neglected. This omission should have a negligible effect on the oscillations provided a Reynolds number $R = \omega|\tilde{x}|a/\nu_0$ and the static part of u are small.

Observations of Forced Shape Oscillations and Rainbow Scattering from Drops

Three groups of experiments on forced resonance will now be summarized. The reader is encouraged to refer to the original papers[3,8,9,28] for details. The first and second made use of properties of scattered light,[28] to detect quadrupole ($\ell = 2$) oscillation in which $\tilde{x}$ was a few μm and smaller. A profile of a drop and the relevant light rays a shown in Fig. 7. Most of the observations were done for drops of benzene and p-xylene in distilled water. The drops were levitated by a continuous acoustic standing wave with a typical frequency of 51 kHz which was << f_c. Their radii were in the range 150 μm to 1.2 mm and the corresponding natural frequencies $\omega*/2\pi$ were predicted to be 1.1 kHz to 50 Hz.

In the first experiments,[3] f_c was typically 679 kHz. When $\tilde{x} = 0$, the interference of rays labeled 0 and 2 in Fig. 7 produces a fine structure in the scattering visible to the eye via a telescope. This structure gives the closely spaced vertical fringes in Fig. 8(a). Conditions on the modulation leading to shape oscillations were mapped by making use of a blurring of the fringes induced by small $\tilde{x}$. The conditions on ω were consistent with the forcing of quadrupole resonance. Large $\tilde{x}$ leading to drop breakup were also observed.

The second group of experiments[8,28] gave quantitative resonance properties. These made use of photometric aspects of the coarse structure in the monochromatic rainbow scattering shown in Fig. 8(a). The "rainbow photometry" technique gave absolute measurements of ξ and relative measurements of $\tilde{x}$ with $|\tilde{x}| < 25$ μm and 0.5 mm < a < 1.2 mm. Here $f_c = 217.5$ kHz and $p_c \leq 70$ kPa. The results are summarized as follows. (i) The dependence of ξ on ω is consistent with Eq. (10c) except that α is larger than calculated and the inferred σ is 4% lower than expected. (ii) With the empirical σ and α, the data give a dependence of ϖ on radius consistent with predictions. (iii) $\tilde{x}$ is maximized when $\omega = \varpi$. (iv) Provided h is held constant, $\tilde{x} \propto p_c^2$ as expected. (v) The empirical α gave Q values which were 70% of the modeled values; however they are consistent with the presence of a film of impurities at the interface. (It is unfortunate that the drops were xylene[8] and benzene.[3] We have recently learned that these liquids almost always form nonideal interfaces with water.) (vi) Uncertainty in a conversion factor precluded the absolute measurement of $\tilde{x}$; however, the estimated $|\tilde{x}|$ are consistent with the R_{20} from Eq. (4). (vii) Empirical Q were typically $= 7$.

In the third group of experiments, Goosby[9] and Marston made hi-speed motion-picture photographs of drops undergoing forced shape oscillations. The drops consisted of a dyed silicone oil with $\nu_i = 2$ cS and $\rho_i = 0.88$ gm/cm^3. They were levitated by a 55 kHz wave in a water-filled resonator consisting of 50 mm x 75 mm glass microscope slides cemented along their long sides. A PZT disc (38 mm dia., 13 mm thick) drove both the 55 kHz wave and a modulated wave with $f_c = 170$ kHz. Drops were levitated and f was adjusted to maximize $|\tilde{x}|$ for quadrupole oscillations apparent to the unaided eye. Figure 9 is taken from a sequence in which every third frame was printed giving a time interval between printed frames of 5.7 ms. Timing marks on the film revealed that $\xi = 90° \pm 9°$ which agree with predictions. This is noteworthy because here $|\tilde{x}|/a = 0.4$ and the Reynolds number $R = 180$. For this measurement kh << 1 and Eqs. (4) and (9) predict that $\hat{x} < 0$. The photographs and timing marks when combined with Eq. (10b) also give $\hat{x} < 0$.with $\ell = 2$ and $m = 0$.

As in Ref. 3, it was observed that oscillation amplitudes could be made large enough to fission the drop. Figure 10 shows the details of the fission process. The time interval between frames was 1.2 ms. This is a new acoustic technique for splitting drops since it relies on the modulation of the radiation pressure. Previous acoustic methods typically depended on transient cavitation to generate shock waves which could split drops.[29]

The Physical Optics of Light Scattering from Bubbles

Unlike the case of scattering from drop-like objects, the physical optics of scattering from bubbles (where the refractive index of the scatterer n_i is less than that of the surroundings n_0) has been explored only recently. This study has emphasized those angular regions of the scattering where diffraction corrects for divergences predicted by geometric optics.[1] These include glory or backscattering,[30] forward scattering,[1] and critical angle scattering.[31,32] The following is only a brief summary; the interested reader should consult Ref. 30-32 and papers cited therein. In this section, ϕ denotes the scattering angle (Fig. 11), λ denotes the wavelength of light within the outer fluid, θ_p denotes the local angle of incidence at the bubble's surface for a ray with p internal chords, and $m \equiv n_i/n_0$. Far-field scattering will be described which is that observed by a camera focused on ∞.

The critical scattering angle, $\phi_c = 2\arccos(m)$, is where the surface reflected ray has an angle of incidence $\theta_0 = \arcsin(m)$. For $\phi \leq \phi_c$, geometric optics predicts that reflection

will be total, however models[31] and Mie theory[32] show that is not the case at ϕ_c due to diffraction. For $\phi < \phi_c (\approx 83°$ for bubbles in water) there is a coarse structure to the scattering due to this diffraction and to the interference with the $p = 1$ ray. This structure (visible in Fig. (8b)) has an angular spacing which is typically $\lesssim (\lambda/a)^{\frac{1}{2}}$ rad. Physical optics models of this structure[32] agree with Mie theory when $a \gtrsim 4\lambda$. For a bubble and drop of the same size, each with $a \gg \lambda$, the bubble's coarse structure is broader than the rainbow's since the latter's quasi-period can be shown from Eq. 5 of Ref. 28 to be $\lesssim (\lambda/a)^{2/3}$ rad. Other photographs of scattering by bubbles[1,31] reveal a fine structure due primarily to the interference of $p = 0$ and 2' rays. Its spacing is typically $\lesssim 0.8 \lambda/a$ radians. Backscattering from bubbles in our model can easily exceed that from a perfectly reflecting sphere of the same size. It has a quasi-periodic structure which is especially regular for the cross-polarized scattering. Observations of this structure agree well with theory.[30] This structure is evident in Fig. 12 as the concentric rings centered in the $\phi = 180°$ direction and spaced at 0.05° intervals.

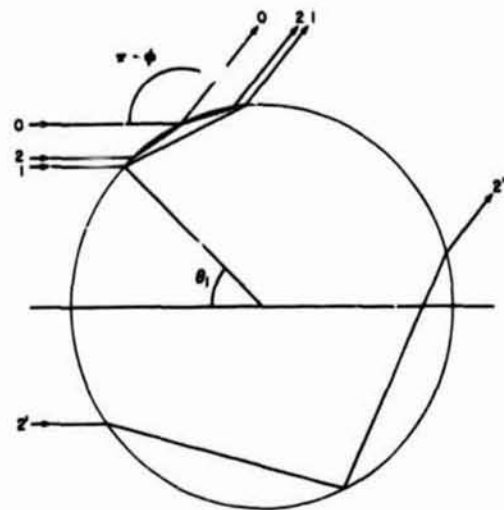Fig. 11. Rays for a bubble in water.

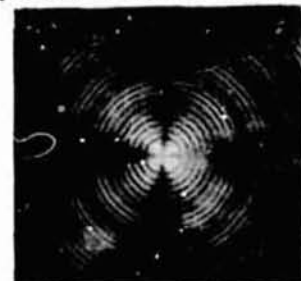Fig. 12. Cross-polarized backscattering from a bubble in si icone oil with a°

Acknowledgments

References

1. P.L. Marston, D.S. Langley, and D.L. Kingsbury, in Proceedings of the IUTAM Symposium on the Mechanics and Physics of Bubbles in Fluids (at press).
2. R.E. Apfel, J. Acoust. Soc. Am. 70, 636-639 (1981).
3. P.L. Marston and R.E. Apfel, J. Colloid Interface Sci. 68, 280-286 (1979).
4. L.A. Crum, J. Acoust. Soc. Am. 50, 157-163 (1971).
5. K. Yosioka and Y. Kawasima, Acustica 5, 167-173 (1955).
6. T. Hasegawa, J. Acoust. Soc. Am. 61, 1445-1448 (1977).
7. A.I. Eller, J. Acoust. Soc. Am. 43, 170-171 (1968).
8. P.L. Marston and R.E. Apfel, J. Acoust. Soc. Am. 67, 27-37 (1980).
9. S.G. Goosby, Photographs of Breakup of Drops Induced by Modulated Radiation Pressure, M.S. dissertation, Washington State University (1981).
10. R.E. Apfel, J. Acoust. Soc. Am. 59, 339-343 (1976).
11. M.A. Weiser and R.E. Apfel, J. Acoust. Soc. Am. (submitted for publication).
12. L.V. King, Proc. Roy. Soc. A137, 212-240 (1934).
13. E. Leung, N. Jacobi, and T. Wang, J. Acoust. Soc. Am. (at press).
14. P.L. Marston, J. Acoust. Soc. Am. 67, 15-26 (1980); (erratum at press).
15. P.L. Marston, S.E. LoPorto, and G.L. Pullen, J. Acoust. Soc. Am. 69, 1499-1501 (1981).
16. R.R. Whymark, Ultrasonics 13, 251-261 (1975); E. Trinh (private communication, 1981).
17. M.E. McIntyre, J. Fluid Mech. 106, 331-347 (1981).
18. F.E. Borgnis, J. Acoust. Soc. Am. 24, 468-469 (1952).
19. B.P. Konstantinov, Zhurnal Tekhnicheskoi Fiziki 9, 226-238 (1939).
20. A.Y. Savelev, Sov. Phys. Acoust. 19, 154-158 (1973).
21. E.M. Herrey, J. Acoust. Soc. Am. 27, 891-896 (1955).
22. F.H. Busse and T.G. Wang, J. Acoust. Soc. Am. 69, 1634-1638 (1981).
23. H. Medwin and I. Rudnick, J. Acoust. Soc. Am. 25, 538-540 (1953).
24. G.I. Taylor, Proc. Roy. Soc. Lond. A291, 159-166 (1966).
25. J.R. Melcher and G.I. Taylor, Annu. Rev. Fluid Mech. 1, 111-146 (1969).
26. K.E. Spells, Proc. Phys. Soc. B65, 541-546 (1952).
27. J. Lighthill, J. Sound Vib. 61, 391-418 (1978).
28. P.L. Marston, Appl. Opt. 19, 680-685 (1980).
29. M.K. Li and H.S. Fogler, J. Fluid Mech. 88, 513-528 (1978).
30. D.S. Langley and P.L. Marston, Phys. Rev. Lett. 47, 913-916 (1981).
31. P.L. Marston, J. Opt. Soc. Am. 69, 1205-1211 (1979); 70, 353(E) (1980).
32. D.L. Kingsbury and P.L. Marston, Appl. Opt. 20, 2348-2350 (1981).